Dyes and Pigments 240 (2025) 112827

Contents lists available at ScienceDirect

Dyes and Pigments

journal homepage: www.elsevier.com/locate/dyepig

Development of a novel near-infrared fluorescent probe based on nile blue for the detection of leucine aminopeptidase as a cancer biomarker

Marcia Domínguez [a,b], David Azorín-Soriano [a,c], Jessie García-Fleitas [a], Jennifer Soler-Beatty [a,c], Andrea Bernardos [a,b,c], Alba García-Fernández [a,b,c], Juan F. Blandez [a,b,d,e,*], Félix Sancenón [a,b,c,d,**], Ramón Martínez-Máñez [a,b,c,d,***]

[a] Instituto Interuniversitario de Investigación de Reconocimiento Molecular y Desarrollo Tecnológico (IDM), Universitat Politècnica de València, Universitat de València, Camino de Vera, s/n, 46022, Valencia, Spain
[b] CIBER de Bioingeniería, Biomateriales y Nanomedicina (CIBER-BBN), Instituto de Salud Carlos III, 28029, Madrid, Spain
[c] Unidad Mixta UPV-CIPF de Investigación en Mecanismos de Enfermedades y Nanomedicina, Universitat Politècnica de València, Centro de Investigación Príncipe Felipe, C/Eduardo Primo Yúfera 3, 46100, Valencia, Spain
[d] Unidad Mixta de Investigación en Nanomedicina y Sensores, Universitat Politècnica de València, Instituto de Investigación Sanitaria La Fe (IISLAFE), Avenida Fernando Abril Martorell 106, 46026 Valencia, Spain
[e] Department of Chemical Engineering and Biotechnology, University of Cambridge, Philippa Fawcett Dr, Cambridge, CB3 0AS, UK

ARTICLE INFO

Keywords:
Near-infrared fluorescent probe
Cancer biomarker
Leucine aminopeptidase
Zwitterionic compounds
Biocompatibility

ABSTRACT

We report herein the design and synthesis of a near-infrared fluorescent probe (**NB–SO_3-Leu**) derived from the Nile Blue (NB) fluorophore scaffold, modified with sulfonic groups to improve solubility and biocompatibility. The mechanism of action of the **NB-SO_3-Leu** probe was successfully validated in the presence of leucine aminopeptidase (LAP), a widely known cancer biomarker. The fluorescence signal of **NB-SO_3-Leu**, which was initially low, increased 4-fold after incubation with the LAP enzyme after 15 min. In addition, the **NB-SO_3-Leu** probe was validated *in vitro* in 4T1 (mouse mammary carcinoma cells), HeLa (human cervical cancer cells), and SK-Mel-103 (human melanoma cells) with high endogenous LAP levels. This work aims to advance in the development of a new generation of reliable and sensitive cancer detection methods.

1. Introduction

Cancer remains one of the world's leading causes of death. Many diagnosed patients fear the lengthy and toxic treatments they may receive, especially in advanced stages where the effectiveness of such treatments may be limited. In fact, once diagnosed, cancers are often found at intermediate or advanced stages using conventional medical tools such as Magnetic Resonance Imaging (MRI), Computed Tomography (CT), Ultrasound (US) and Photoacoustic Imaging (PA) (Fig. 1) [1–3]. These methods often lack the sensitivity to detect small tumors or early tissue changes, which can lead to late diagnosis. In addition, these techniques have limitations due to the frequent need for additional invasive procedures, such as biopsies [4]. Some methods, such as CT, use ionizing radiation, with the potential side effects this can cause [5].

Abbreviations: (WHO), World Health Organization; (NB), Nile Blue; (LAP), Leucine Aminopeptidase; (MRI), Magnetic Resonance Imaging; (CT), Computed Tomography; (US), Ultrasound; (PA), Photoacoustic Imaging; (NIR), Near-Infrared; (BODIPYs), Boron-Dipyrromethenes; (RES), Reticuloendothelial System; (ATCC), American Type Culture Collection; (DMEM), Dulbecc's Modified Eagle Medium; (FBS), Fetal Bovine Serum; (S_N2) Reaction, Bimolecular Nucleophilic Substitution; (TFA), Trifluoroacetic Acid; (HPLC-MS), High-Performance Liquid Chromatography-Mass Spectrometry.

* Corresponding author. Instituto Interuniversitario de Investigación de Reconocimiento Molecular y Desarrollo Tecnológico (IDM), Universitat Politècnica de València, Universitat de València, Camino de Vera, s/n 46022, Valencia, Spain.
** Corresponding author. Instituto Interuniversitario de Investigación de Reconocimiento Molecular y Desarrollo Tecnológico (IDM), Universitat Politècnica de València, Universitat de València, Camino de Vera, s/n 46022, Valencia, Spain.
*** Corresponding author. Instituto Interuniversitario de Investigación de Reconocimiento Molecular y Desarrollo Tecnológico (IDM), Universitat Politècnica de València, Universitat de València, Camino de Vera, s/n 46022, Valencia, Spain.
E-mail addresses: juan.blandez@uv.es (J.F. Blandez), fsanceno@upvnet.upv.es (F. Sancenón), rmaez@qim.upv.es (R. Martínez-Máñez).

https://doi.org/10.1016/j.dyepig.2025.112827
Received 5 March 2025; Received in revised form 3 April 2025; Accepted 9 April 2025
Available online 10 April 2025

Additionally, these methods provide static images at specific points in time and do not allow dynamic, real-time monitoring of tumor progression [6]. These drawbacks underscore the importance of developing minimally invasive detection procedures to enhance cancer diagnosis and treatment monitoring.

As an alternative, techniques based on the evaluation of cancer-related biomarkers are emerging as the most promising for detection and treatment monitoring [7–12]. A large number of potential cancer biomarkers have been described [13,14]. Among them, overexpressed enzymes are gaining interest because of the important role they play in both physiological and pathological processes. The levels of enzymes, their location (intra- or extracellular), or their accumulation at the subcellular level, can determine the presence of an abnormal state of homeostasis. The importance of deregulated enzymes in the cancer process underlines the need to develop techniques that allow their easy, and less invasive detection. In this respect, developing fluorescent probes both for imaging and real-time monitoring of tumor progression through functional readouts of specific biomolecules is gaining attention. Fluorescence techniques have high sensitivity, show good spatio-temporal resolution and are usually inexpensive [15–17].

Research efforts in recent years have focused on developing fluorescent probes in the near-infrared (NIR) wavelength range (650–900 nm). Despite the progress, there are still some challenges to be solved. For example, molecules such as boron-dipyrromethenes (BODIPYs), cyanines, and coumarins with emissions in the NIR window are usually based on fused aromatic rings, which drastically reduces their solubility in biofluids and increases their toxicity [18–26]. Moreover, most of the developed probes (such as fluorophores conjugated to nanoparticles, quantum dots, or gadolinium-based contrast agents) are mainly eliminated by the reticuloendothelial system (RES), which could lead to their accumulation in the liver and spleen, with the subsequent potential organ toxicity and side effects, which is also an important drawback [27,28]. As an alternative, the presence of zwitterionic groups in the structure of a fluorophore has been described to increase biocompatibility by favoring its renal clearance, reducing the binding of the fluorophore to proteins and non-specific uptake in normal tissues [29,30]. Zwitterionic compounds are molecules that contain functional groups with opposite charges, i.e. they have both a positive and a negative charge on different atoms, but together they are electrically neutral [31,32]. This characteristic gives them high water solubility and other unique features such as a low tendency to aggregate and high chemical stability. Zwitterionic compounds are particularly useful in biological and medical applications due to their biocompatibility and ability to interact favorably with biological components.

In line with the ideas outlined above, and intending to develop systems that allow cancer detection without requiring expensive equipment or highly qualified personnel, we report here the synthesis and characterization of the fluorescent molecular probe, **NB-SO_3-Leu**. This probe is based on the Nile Blue (NB) fluorophore chemically modified with a sulfonic group to form a zwitterionic structure. NB offers several significative advantages as a fluorophore [33–35] due to its remarkable properties as *in vivo* imaging agent [36]. Its strong fluorescence enables sensitive and accurate detection of biological molecules, facilitating detailed visualization of specific biomarkers in cells and tissues. In addition, its photochemical stability ensures that the images obtained are long-lasting, which is ideal for studies that require prolonged observation times. However, NB presents problems related to its limited solubility in aqueous environments and can therefore accumulate in tissues and organs, causing undesirable side effects that can limit its use in certain experimental contexts. The inclusion of sulfonic groups onto the NB framework and the zwitterionic structure of the modified fluorophore will increase its solubility in aqueous environments diminishing deleterious side effects. Moreover, it has been reported that increased solubility favors rapid elimination by the reticuloendothelial system (RES), reducing the half-life of the molecule in the body and preventing its accumulation in sensitive tissues [37,38].

On the other hand, the overexpression of aminopeptidases has been linked to cancer progression and malignancy [39–44]. Targeting the hydrolytic features of aminopeptidases represents a promising approach for cancer imaging, and different fluorogenic probes have been developed in recent years due to its relevance [45–48]. Taking into account these facts, we modified the structure of NB-SO_3 fluorophore with a leucine residue in order to prepare a molecular probe for leucine aminopeptidase (LAP) detection (**NB–SO_3-Leu**). Specifically, LAP was chosen to validate the function of the probe because it is an enzyme that catalyzes the hydrolysis of peptidic bonds in which the amino group at the N-terminal position of a peptide or protein is a leucine [49,50]. Elevated levels of LAP have been reported in tissue from ovarian

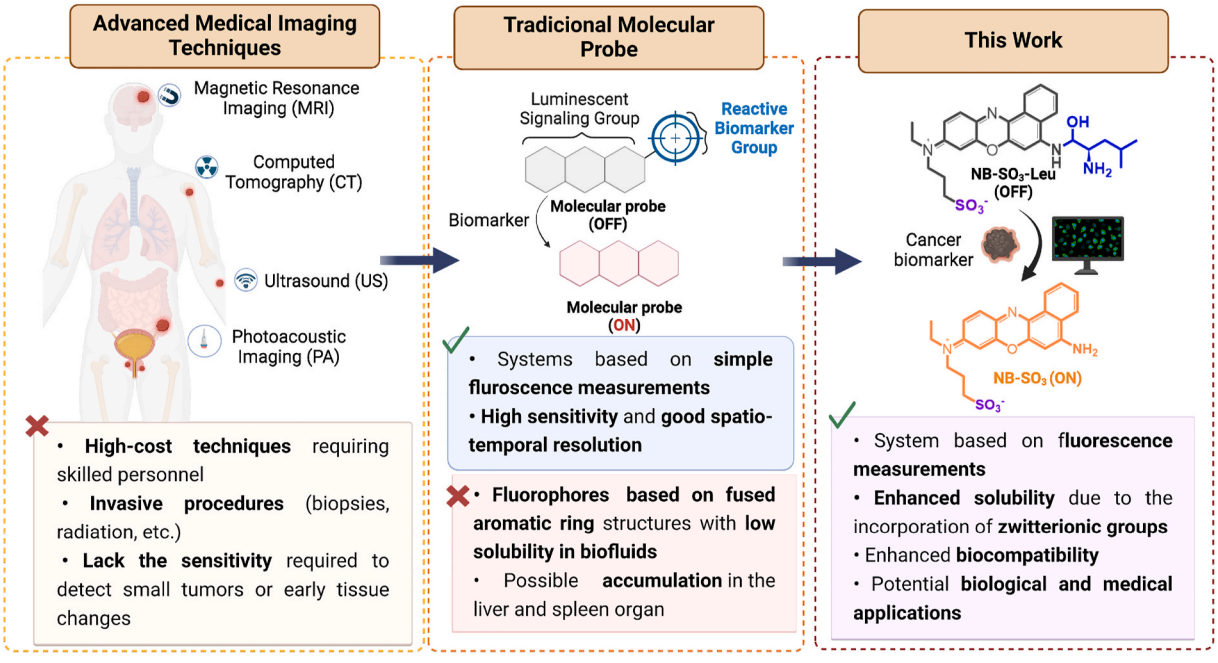

Fig. 1. Different protocols developed for the detection of cancer biomarker including the fluorescent probe **NB-SO_3-Leu** proposed in the present work.

epithelial cancer, breast cancer, liver cancer and skin cancer (particularly melanoma) [51–54]. Although fluorescent probes have been developed for the *in vitro* and *in vivo* detection of elevated LAP (Table S1), most of these probes present some of the previously mentioned issues, such as poor solubility and unwanted accumulation [55–62].

This work represents progress and lays the groundwork for developing a new generation of molecular sensors for cancer detection. The developed **NB-SO_3-Leu** is designed in such a way that shows a very weak emission (OFF state) and, in the presence of LAP, the highly NB-SO_3 fluorophore is produced (ON state). Prospective *in vitro* studies with 4T1 mouse mammary carcinoma cells, HeLa human cervical cancer cells and SK-Mel-103 human melanoma cells with high levels of endogenous LAP enzyme indicate the possibility of using this type of molecular probe for cancer detection protocols. In addition, the **NB-SO_3-Leu** probe addresses a critical challenge in the field of molecular sensors of minimizing side effects due to possible accumulation. The use of such molecular sensors opens new possibilities for cancer detection as NB-SO_3 fluorophore could be easily modified and adapted to detect different protease activity or enzymatic activity associated as cancer biomarkers.

2. Experimental

2.1. Materials and methods

3-aminophenol, iodoethane, 1,3-propanesultone, 2-ethoxy-1-ethoxycarbonyl-1,2-dihydroquinoline, *N*,*N*-dimethylformamide (DMF), triethylamine, *N*-(tert-butoxycarbonyl)-L-leucine (Boc-Leu-OH), $NaNO_2$, K_2CO_3, $FeCl_3$, $CaCl_2$, $MnCl_2$, $MgCl_2$, H_2O_2, glutathione, cysteine, arginine, glycine, bestatin, monoamine oxidase A from *baculovirus* infected BTI insect cells (MAO-A), γ-glutamyltransferase from porcine kidney, nitroreductase from *Escherichia coli* and leucine aminopeptidase from porcine kidney (LAP) were obtained from Sigma-Aldrich. ^1H and ^{13}C NMR spectra were recorded on a Bruker FT-NMR Avance 400 (Ettlingen, Germany) spectrometer at 300 K. Fluorescence spectroscopy was carried out in a JASCO spectrofluorometer FP-8500 and absorption spectra were collected in a JASCO V-650 spectrophotometer. HPLC-MS was recorded with an Agilent 1620 Infinity II HPLC coupled to a mass spectrometer Agilent Ultivo equipped with a triple QTOF detector. PuriFlash XS 520 Plus was used for purification.

2.2. Synthesis of NB-SO_3

The synthesis of products **1**, **2** and **3** were adapted from *Chem. Eur. J.* **2009**, *15*, 418–442.

2.2.1. Synthesis of (3-ethylamino) phenol **(1)**

3-aminophenol (2.10 g, 19.3 mmol) and K_2CO_3 (2.52 g, 18.2 mmol) were mixed in a round bottom flask under argon atmosphere and dissolved in anhydrous DMF (10 mL). The reaction mixture was stirred for 15 min under argon atmosphere at room temperature until complete solution of reagents. Then, iodoethane (1.5 mL, 18.7 mmol) was added dropwise (0.05 mL·min^{-1}) for 30 min at 100 °C. After complete addition, the whole reaction mixture was stirred 2 h at 100 °C. The reaction is then cooled to room temperature and K_2CO_3 removed by filtration. Solvent was removed under reduced pressure and the obtained oil resuspended in 10 mL water and extracted 2 times with ethyl acetate. The solvent was eliminated under vacuum. The residue was purified by column chromatography on silica gel (hexane-ethyl acetate 5:1 v/v as eluent) to obtain product **1** as brown oil (82 % yield). ^1H NMR (400 MHz, $CDCl_3$) δ (ppm): 7.02 (t, $J = 8.0$ Hz, 1H), 6.23 (m, 2H), 6.10 (s, 1H), 4.17 (qd, $J = 7.2$, 3.7 Hz, 1H), 3.07 (m, 2H), 1.20 (t, $J = 7.1$ Hz, 3H). ^{13}C NMR (101 MHz, $CDCl_3$) δ (ppm): 156.97, 149.73, 130.19, 106.23, 105.24, 100.79, 38.80, 14.63.

2.2.2. Synthesis of (3-(ethyl(3-hydroxyphenyl)amino)propane-1-sulfonate) **(2)**

Compound **1** (316.8 mg, 2.30 mmol) and 1, 3-propanesultone (336.1 mg, 2.75 mmol) were mixed in a bottom round flask of 10 mL and dissolved in isopropanol (3 mL). The reaction mixture was heated under reflux at 90 °C for 3 h. The appearance of the reaction mixture changes rapidly to a light pink color, followed by the appearance of a white precipitate. Finally, the reaction is cooled to room temperature. Precipitate was isolated by filtration and washed with cold isopropanol. The solid is collected and dried overnight under vacuum. Compound **2** was used in the next synthetic step without further purification (52 % yield). ^1H NMR (400 MHz, D_2O) δ (ppm): 7.52 (t, $J = 8.2$ Hz, 1H), 7.12–7.08 (m, 2H), 7.04 (t, $J = 2.3$ Hz, 1H), 3.80–3.74 (m, 2H), 3.68 (q, $J = 7.2$ Hz, 2H), 2.92 (t, $J = 7.2$ Hz, 2H), 1.97 (q, $J = 7.6$ Hz, 2H), 1.16 (t, $J = 7.2$ Hz, 3H). ^{13}C NMR (101 MHz, D_2O) δ (ppm): 158.90, 137.66, 133.04, 117.73, 113.71, 109.04, 56.38, 54.38, 47.57, 20.40, 8.91.

2.2.3. Synthesis of (3-(ethyl (3-hydroxy-4-nitrophenyl) amino) propane-1-sulfonate) **(3)**

Compound **2** (193.2 mg, 0.75 mmol) was dissolved in 1 mL of HCl–H_2O 13:7 v/v and cooled in an ice bath. Then, a $NaNO_2$ solution (60 mg, 0.87 mmol) in H_2O (1.2 mL) was added dropwise to reaction mixture. The color changes immediately to bright yellow. The stirring was kept for 3 h. Then, the reaction mixture was filtered and the solvent removed under reduced pressure to obtain compound **3** as a black-brownish solid and employed immediately in the next step (91 % yield).

2.2.4. Synthesis of NB-SO_3

3 (200 mg, 0.66 mmol) and 1-naphthylamine (95 mg, 0.66 mmol) were mixed in a round bottomed flask under argon atmosphere and dissolved in anhydrous DMF (5 mL). The reaction mixture was stirred at 90 °C under argon atmosphere overnight. The solvent was eliminated under vacuum. The crude reaction was purified through a Soxhlet extraction to obtain NB-SO_3 as a blue solid (68 % yield). ^1H NMR (400 MHz, MeOD) δ (ppm): 8.85 (d, $J = 8.2$ Hz, 1H), 8.26 (d, $J = 8.2$ Hz, 1H), 7.89–7.70 (m, 3H), 7.25 (d, $J = 9.4$ Hz, 1H), 6.95 (s, 1H), 6.82 (s, 1H), 3.73 (t, $J = 7.7$ Hz, 2H), 3.68–3.60 (m, 2H), 2.85 (t, $J = 6.8$ Hz, 2H), 2.08 (d, $J = 14.7$ Hz, 2H), 1.29–1.15 (m, 3H). ^{13}C NMR (101 MHz, MeOD) δ (ppm): 148.18, 147.41, 140.10, 136.03, 132.87, 130.28, 130.18, 130.00, 129.77, 128.83, 128.72, 127.91, 126.87, 124.41, 122.46, 97.34, 96.11, 45.49, 25.69, 10.70. HR-MS: Theoretical ($M + H^+$): 411.47 m/z; Experimental ($M + H^+$): 412.13 m/z.

2.2.5. Synthesis of **NB-SO_3-Leu**

Boc-Leu-OH (138.8 mg, 0.6 mmol), triethylamine (68.2 μL, 0.49 mmol) and 2-ethoxy-1-ethoxycarbonyl-1, 2-dihydroquinoline (123.6 mg, 0.49 mmol) were mixed in a round bottom flask under argon atmosphere and dissolved in anhydrous DMF (5 mL). The reaction mixture was stirred at room temperature for 1 h. Then, NB-SO_3 (200 mg, 0.49 mmol) dissolved in anhydrous DMF (2 mL) was added dropwise to the reaction mixture. The crude was heated at 70 °C for 32 h. After this time trifluoroacetic acid (TFA) dilution (5 mL DMF and 0.75 mL TFA) was added to the reaction mixture and stirred for 24 h. The solvent was eliminated under vacuum. The product was purified in the PuriFlash XS 520 Plus using a PF-30C18HP-F0004 column (hexane-ethyl acetate 95:5 v/v as eluent, 5.0 mL·min^{-1} of flow rate) to obtain **NB-SO_3-Leu** probe as purple solid (55 % yield). ^1H NMR (400 MHz, DMSO) δ (ppm): 9.41 (s, 1H), 9.09 (dd, $J = 4.7$, 1.7 Hz, 1H), 8.73 (dd, $J = 8.4$, 1.6 Hz, 1H), 8.15 (d, $J = 8.1$ Hz, 2H), 7.93 (ddd, $J = 8.6$, 7.0, 1.5 Hz, 1H), 7.80–7.74 (m, 2H), 3.09 (qd, $J = 7.3$, 4.4 Hz, 6H), 1.36 m, 4H), 1.18 (t, $J = 7.3$ Hz, 9H), 0.88–0.84 (m, 2H). ^{13}C NMR (101 MHz, DMSO) δ (ppm)158.54, 158.18, 148.48, 143.65, 140.25, 131.55, 128.54, 128.16, 127.80, 125.65, 121.71, 117.60, 114.68, 77.84, 45.67, 45.62, 28.16, 24.30, 23.07, 22.94, 21.48, 8.52. HRMS: Theoretical ($M + H^+$): 524.636 m/z. Experimental ($M + H^+$): 525.216 m/z.

2.3. General procedure for LAP detection

Fluorescence emission measurements of **NB-SO$_3$-Leu** were carried out with 1 μL of the probe from a stock solution (1.0×10^{-3} M in DMSO), followed by addition of LAP solution in PBS (10 mM, pH 7.4). Final volume was adjusted to 200 μl with PBS at pH 7.4. After incubation at 37 °C for 15 min in a thermostat, solution was transferred to a quartz cell of 1 cm optical length to measure the fluorescence (λ_{exc} = 630 nm). Control samples, without LAP enzyme, were prepared and measured under the same conditions.

2.3.1. HPLC measurements of LAP-induced hydrolysis of NB-SO$_3$

Pure **NB-SO$_3$-Leu** probe and NB-SO$_3$ fluorophore samples were taken from a 1.0×10^{-3} M stock solution to obtain a final concentration of 5 μM. The hydrolysis sample chromatogram was recorded 10 min after incubating **NB-SO$_3$-Leu** probe (5 μM) with LAP enzyme (750 ng·mL^{-1}). HPLC chromatograms were obtained using a Hypersil Gold CN column, flow rate of 1.8 mL·min^{-1}, with buffer (0.2 M KH_2PO_4 solution, pH = 3.0 ± 0.1)-acetonitrile-ethanol (90:10:2 v/v/v) at 17 min. Additionally, chromatograms of NB-SO$_3$ and **NB-SO$_3$-Leu** alone were obtained under the same experimental conditions.

2.4. Cell culture

4T1, HeLa, and SK-Mel-103 cell line was purchased from the American Type Culture Collection (ATCC) and cultured in Dulbecco's Modified Eagle Medium (DMEM) supplemented with 10 % Fetal bovine serum (FBS). Cells were maintained in a 20 % O_2 and 5 % CO_2 atmosphere at 37 °C.

2.4.1. Western blot assays

To determine the levels of LAP enzyme in 4T1, HeLa and SK-Mel-103 cells, whole cell extracts were obtained by using lysis buffer (25 mM Tris-HCl pH 7.4, 1 mM EDTA, 1 % SDS, plus protease and phosphatase inhibitors). Cell lysates were resolved in 12 % SDS-PAGE gels, transferred to nitrocellulose membranes, blocked with 5 % non-fat milk, and incubated overnight with the primary antibody for LAP (#PA5-80533, Invitrogen). Besides, GAPDH (#14C10 from Cell Signaling) was used as reference protein for normalization. Then, membranes were washed and probed with the secondary antibody conjugated to horseradish peroxidase, anti-rabbit IgG peroxidase antibody (#A6154, Sigma) for enhanced chemiluminescence detection (Amersham Pharmacia Biotech).

2.4.2. In vitro cytotoxicity studies

For the *in vitro* cytotoxicity studies 4T1, HeLa and SK-Mel-103 cells were seeded in a 96-well plate (5.000 cells/well) and incubated for 24 h. Then, the cells were incubated with varying concentrations of the **NB-SO$_3$-Leu** probe (diluted in DMEM) for 24 h. The cell viability was determined by WST-1 reagent, which was added for 30 min, and then absorbance was measured at 450 nm in a PerkinElmer life sciences Wallac Victor2TM spectrophotometer.

2.4.3. Confocal in vitro experiments

4T1, HeLa and SK-Mel-103 cells were seeded in a cover slip in a 6-well plate at 250,000 of cells·mL^{-1}. After 24 h, some cells were treated with a broad-spectrum protease inhibitor cocktail (Sigma, P1860, 1:200) for 1 h, whereas others remained untreated. After that, cells were washed and incubated with **NB-SO$_3$-Leu** (10 μM) for 15 min. Then, cells were washed, and coverslips were mounted to confocal visualization. Hoechst 33342 was added at 2 μg·mL^{-1} for nuclei staining. Confocal images were acquired in a Leica TCS SP8 AOBS confocal microscope (λ_{exc} = 638 nm; λ_{em} = 656–781 nm). Images were quantified using Image J software.

3. Results and discussion

Synthesis and characterization of NB-SO$_3$-Leu. NB-SO$_3$ fluorophore was synthesized following the procedure shown in Fig. 2a. In the first step, 3-aminophenol was alkylated with iodoethane by a bimolecular nucleophilic substitution (S_N2) reaction, yielding (3-ethylamino) phenol (**1**). Next, compound **1** reacted with 1,3-propanesultone, again by an S_N2 reaction, yielding the sulfonic acid derivative **2**. Then, in the third step, compound **2** was nitrosylated with sodium nitrite to obtain product **3**. Finally, NB-SO$_3$ fluorophore was obtained by a condensation reaction between **3** and 1-naphthylamine (68 % global yield).

In addition, **NB-SO$_3$-Leu** probe was synthesized using a two-step protocol detailed in Fig. 2b. In the first step, tert-butyloxycarbonyl-L-leucine (Boc-Leu-OH) was covalently linked, through the formation of an amide bond, with the NB-SO$_3$ fluorophore. Then, in a second step, the tert-butyloxycarbonyl (Boc) protecting group was removed with trifluoroacetic acid (TFA), yielding **NB-SO$_3$-Leu** (55 % global yield). NB-SO$_3$ fluorophore, **NB-SO$_3$-Leu** probe and the intermediates were characterized by ^{1}H NMR, ^{13}C NMR and HRMS (Figs. S1–S6).

Photophysical characterization of the enzymatic reaction. NB-SO$_3$-Leu was designed in such a way that LAP enzyme hydrolyses the leucine residue yielding the highly emissive NB-SO$_3$ fluorophore (Fig. 3a). Dealing with the photophysical features of NB-SO$_3$, PBS-DMSO 99:1 v/v (pH 7.4) solutions of the fluorophore (5 μM) showed an emission band at 660 nm (λ_{ex} = 630 nm, $\Phi_{\text{NB-SO3}}$ = 0.023, See Supplementary Information for calculation details). Besides, the emission of NB-SO$_3$ (5 μM in PBS-DMSO, 99:1 v/v) remained unchanged in the 5.0–9.0 pH interval (Fig. S7), which is a suitable characteristic for its use in biological media. In marked contrast, PBS-DMSO 99:1 v/v (pH 7.4) solutions of **NB-SO$_3$-Leu** probe (5 μM) show a very weak emission band at ca. 660 nm (λ_{exc} = 630 nm, $\Phi_{\text{NB-SO3-Leu}}$ = 0.003, See Supplementary Information, Table S2). This reduced emission of the **NB-SO$_3$-Leu** probe is ascribed to the presence of a leucine residue directly linked, through an amide bond, with the NB-SO$_3$ fluorophore, which quenches its emission through an internal charge transfer (ICT) effect [63].

To determine the ability of the **NB-SO$_3$-Leu** probe for LAP enzyme detection, further fluorescence studies were carried out. As stared above, it is expected that LAP hydrolysis of weakly emissive **NB-SO$_3$-Leu** would induce the appearance of a marked emission due to NB-SO$_3$ fluorophore generated after detachment of leucine residue from the probe (Fig. 3a). For this purpose, emission of **NB-SO$_3$-Leu** in PBS-DMSO 99:1 v/v was monitored in the presence and absence of the LAP enzyme. As could be seen in Fig. 3b, a marked 4-fold emission enhancement at ca. 660 nm (λ_{exc} = 630 nm) was observed. This emission enhancement was ascribed to the proposed mechanism, in which LAP-induced hydrolysis of **NB-SO$_3$-Leu** probe yielded the emissive NB-SO$_3$ fluorophore.

LAP-induced enzymatic hydrolysis of **NB-SO$_3$-Leu** probe was also corroborated through HPLC studies (Fig. 3c). As could be seen in Fig. 3c, HPLC chromatograms of **NB-SO$_3$-Leu** probe (5 μM) in PBS-DMSO 99:1 v/v (pH 7.4) showed a single peak at 12.3 min. However, after probe incubation with LAP enzyme for 10 min, a marked reduction of the **NB-SO$_3$-Leu** peak and the appearance of a new signal at 17.4 min was observed (see also Fig. 3c), which corresponds to the NB-SO$_3$ fluorophore.

Changes in fluorescence emission intensity of **NB-SO$_3$-Leu** probe were also monitored in the presence of increasing concentrations of LAP enzyme (0–750 ng·mL^{-1}). Samples were incubated with LAP for 15 min at 37 °C before monitoring the emission intensity at 660 nm. The fluorescence emission recorded at 660 nm (λ_{exc} = 630 nm) was enhanced as a function of the increase in the amount of the LAP enzyme added (Fig. 3d). The calibration curve obtained from these data exhibits a linear range from 0 to 40.0 ng·mL^{-1} of LAP (R^2 = 0.97) with LOD 7.2 ng·mL^{-1} and a LOQ of 21.8 ng·mL^{-1} (Equation S(2)) (Fig. 3e). LOD values of **NB-SO$_3$-Leu** are comparable to, and in some cases even lower than those reported for other probes in the literature (Table S1). This

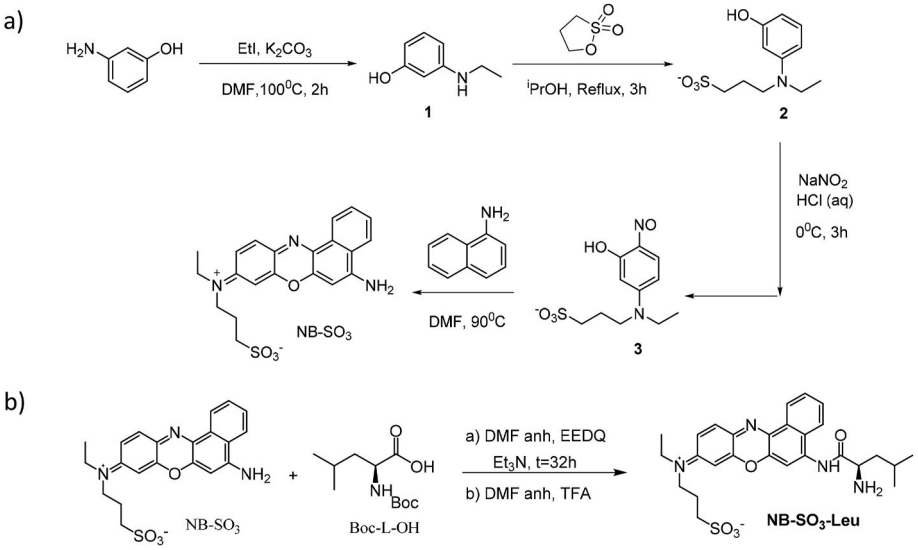

Fig. 2. (a) Synthesis of NB-SO_3 fluorophore. (b) Synthetic sequence used to prepare **NB-SO_3-Leu** probe.

LOD indicates that LAP can be detected at relatively low concentrations. However, although some studies suggest that LAP levels are often correlated with the presence and progression of cancer, there are few data detailing LAP concentrations at all stages of disease, indicating that further research is needed to establish standardized benchmarks for LAP concentration in various types of cancer and their respective progressions.

On the other hand, a kinetic study of **NB-SO_3-Leu** probe hydrolysis in the presence or absence of the LAP enzyme was carried out (Fig. 3f and Fig. S8). The weak fluorescence emission of the **NB-SO_3-Leu** probe in PBS-DMSO 99:1 v/v at pH 7.4 remained practically unchanged in the absence of LAP enzyme. However, **NB-SO_3-Leu** probe incubation with LAP enzyme (750 ng mL^{-1}) shows a progressive fluorescence enhancement centered at 660 nm that reached the maximum value 15 min after enzyme addition. Subsequently, the enzyme kinetics between **NB-SO_3-Leu** and LAP were investigated (Fig. S9). The maximum velocity (V_{max}) and Michaelis constant (K_m) were determined to be 9.26 μM•min^{-1} and 2.40 μM, respectively. The Km value of this probe is lower than those reported for previously described LAP-activatable molecular probes (Table S1). A lower Km suggests that the probe binds more efficiently to LAP, requiring a lower concentration to reach half V_{max} [64].

Taking into account the satisfactory results obtained, the **NB-SO_3-Leu** probe was validated in the presence of several potentially interfering species (including cations, small biomolecules and other enzymes) [65]. Only in the presence of LAP enzyme, a marked emission at 660 nm was recorded (Fig. 3g). To further evaluate the detection mechanism, the **NB-SO_3-Leu** probe was incubated with LAP in the presence of a protease inhibitor cocktail consisting of serine, cysteine, aspartic proteases and aminopeptidase inhibitors. Strong fluorescence is recorded at 660 nm after incubation of the probe with the LAP enzyme. However, this signal is reduced to 2.4-fold when the probe is incubated with LAP enzyme in the presence of a protease inhibitor cocktail (Fig. 3h). The decrease in fluorescence in the presence of the inhibitor cocktail confirms that the fluorescent activation of **NB-SO_3-Leu** is due to the enzymatic activity of LAP, thus validating the proposed detection mechanism for elevated LAP levels using the **NB-SO_3-Leu** probe.

Once the efficacy of the mechanism has been demonstrated in buffered solutions, the **NB-SO_3-Leu** probe was validated in Dulbecco's Modified Eagle Medium (DMEM) a more competitive environment similar to cell cytoplasm. The aim was to verify how many proteolytic enzymes, i.e. enzymes whose function is protein degradation, could interfere in the observed emission signal. To this end, the **NB-SO_3-Leu** probe was incubated in the presence of interfering alanine aminopeptidase, pronase and protease in DMEM supplemented with 10 % Fetal bovine serum (FBS) (Fig. 4a). In this context, the greatest variation in fluorescence was observed when the probe was incubated in the presence of LAP, confirming the initially proposed hydrolysis mechanism.

***In vitro* validation of the NB-SO_3-Leu probe**. Encouraged by the satisfactory results obtained with the **NB-SO_3-Leu** probe for LAP detection, *in vitro* studies were carried out using 4T1, HeLa and SK-Mel-103 cells, which have been reported to have high levels of endogenous LAP enzyme [66,67]. LAP enzyme expression in these cell lines was corroborated by Western blot assays (Fig. 4b). In addition, toxicity studies demonstrated the biocompatibility of the **NB-SO_3-Leu** probe in the three cell lines tested after 24 h of incubation, even at high concentrations. (Fig. 4c). In addition, confocal microscopy assays were carried out to assess the activation of the **NB-SO_3-Leu** probe in 4T1, HeLa and SK-Mel-103 cells. A strong fluorescence signal was observed in 4T1, HeLa and SK-Mel-103 cells incubated with the **NB-SO_3-Leu** probe, whereas when cells were treated with a protease inhibitor cocktail before incubation with the **NB-SO_3-Leu** probe, a ca. 0.5-fold decrease in fluorescence intensity was observed (Fig. 4d and e).

NB-SO_3-Leu was confirmed as a suitable molecular probe for the imaging and detection of LAP demonstrating its potential as a powerful tool for minimally invasive cancer diagnosis. The probe's ability to respond to elevated LAP levels in 4T1, HeLa and SK-Mel-103 cells underscores its utility in real-time imaging applications. The significant fluorescence activation observed in the presence of LAP indicates a promising avenue for the early detection of melanoma, breast cancer and potentially other cancers characterized by similar enzyme profiles.

4. Conclusions

One major objective in health is the development of new diagnostic technologies that are both affordable and simple to use. This works represents and advance in the field by designing a fluorogenic molecular probe with increased solubility that is rapidly activated in cells and tissues in the presence of a certain biomarker. For this purpose, the synthesis and characterization of the **NB-SO_3-Leu** probe was performed, whose mechanism was validated in the presence of the LAP enzyme as cancer biomarker. The enzyme activity is monitored by following the fluorescent signal of NB-SO_3 fluorophore, which is produced after hydrolysis of the originally low-emissive **NB-SO_3-Leu** probe.

Initially, **NB-SO_3-Leu** probe was validated in buffered solutions, demonstrating its ability to respond to high levels of LAP enzyme by

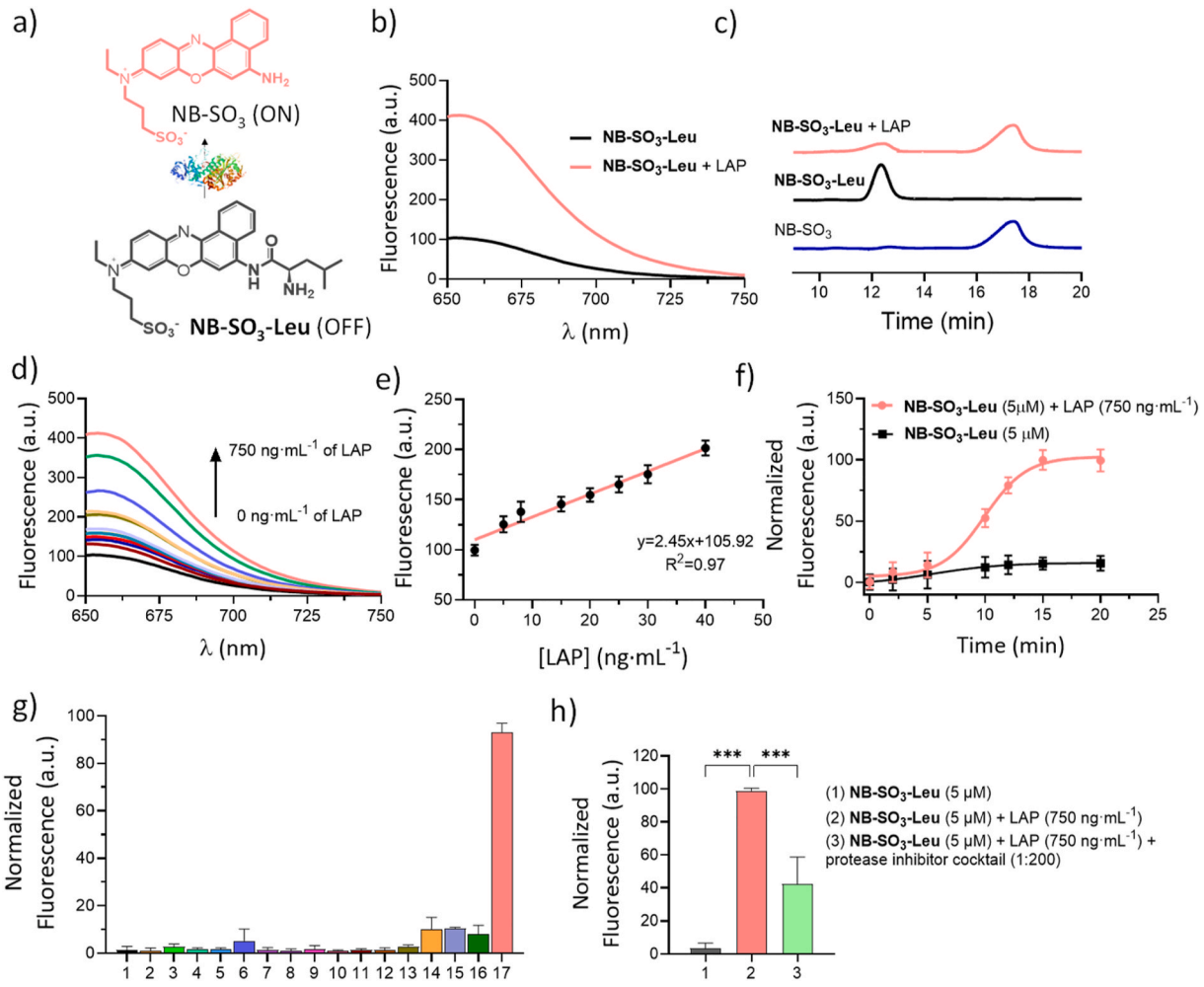

Fig. 3. (a) LAP-induced hydrolysis of **NB-SO$_3$-Leu** probe. (b) Fluorescence emission of **NB-SO$_3$-Leu** (5 μM) + LAP (2.34 μM ≈ 750 ng·mL^{-1}) (red curve) and **NB-SO$_3$-Leu** (5 μM) (black curve) at 660 nm in PBS-DMSO 99:1 v/v at pH 7.4 (λ_{exc} = 630 nm), after 15 min upon LAP enzyme addition. (c) Chromatograms of **NB-SO$_3$-Leu** (5 μM) + LAP (750 ng·mL^{-1}) after 10 min upon enzyme incubation (red curve), **NB-SO$_3$-Leu** (black curve) and NB-SO$_3$ (5 μM) (blue curve) in PBS-DMSO 99:1 v/v at pH 7.4. Conditions: ODS Hypersil column, 1.8 mL·min^{-1}, Buffer (0.2 M of KH_2PO_4 solution, pH = 3 ± 0.1)-MeCN-Ethanol (90:10:2 v/v/v) elution at 20 min. (d) Fluorescence emission spectra of **NB-SO$_3$-Leu** (5 μM) in PBS-DMSO 99:1 v/v, pH 7.4 in the presence of different concentrations of LAP enzyme (0–750 ng·mL^{-1}). (e) Calibration curve of **NB-SO$_3$-Leu** (5 μM) at different APN concentrations in PBS-DMSO 99:1 v/v at pH 7.4. Fluorescence measurements were taken 15 min after LAP addition. Error bars are expressed as 3σ for three independent experiments. (f) Fluorescence of **NB-SO$_3$-Leu** (5 μM) in (PBS–DMSO 99: 1 v/v, pH 7.4) at different time points in the absence (black curve) and in the presence of LAP enzyme (750 ng·mL^{-1}) (red curve). (g) Fluorescence emission of **NB-SO$_3$-Leu** (5 μM) in PBS-DMSO 99:1 v/v at pH 7.4 in the presence of different interferents at 660 nm (excitation at 630 nm): 1. Blank (5 μM); 2. Ca^{2+} (1 mM); 3. Fe^{3+} (1 mM); 4. Mg^{2+} (1 mM); 5. Mn^{2+} (1 mM); 6. H_2O_2 (10 mM); 7. Glutathione (1 mM); 8. Cysteine (1 mM); 9. Monoamine oxidase-A (100 mg•mL^{-1}); 10. α-Glutamyltransferase (100 mg·mL^{-1}); 11. Nitroreductase (100 mg·mL^{-1}); 12. Arginine (1 mM); 13. Glycine (1 mM); 14. Pronase (mg·mL^{-1}); 15. Protease (mg·mL^{-1}); 16. Alanine aminopeptidase (APN) (mg·mL^{-1}); 17. LAP (750 ng·mL^{-1}). (h) Fluorescence at 660 nm of: (1) **NB-SO$_3$-Leu** (5 μM), (2) **NB-SO$_3$-Leu** (5 μM) + LAP (750 ng·mL^{-1}) and (3) **NB-SO$_3$-Leu** (5 μM) + LAP (750 ng·mL^{-1}) + protease inhibitor cocktail (1:200) in PBS-DMSO 99:1 v/v at pH 7.4. Error bars are expressed as 3σ for three independent experiments. Values are expressed as mean ± SD. Statistical analysis was assessed by applying One-way Anova (****p < 0.0001, **p < 0.0050). (For interpretation of the references to color in this figure legend, the reader is referred to the Web version of this article.)

significantly increasing the fluorescent signal. Subsequently, the validation was extended to a more competitive medium (DMEM with FBS), representative of a biological environment. To assess the robustness of the **NB-SO$_3$-Leu** probe, assays were performed in the presence of other potentially interfering proteolytic enzymes, such as alanine aminopeptidase, pronase and protease, with a more pronounced variation in fluorescence observed in the presence of LAP enzyme. Finally, confocal microscopy assays confirmed the capability of the **NB-SO$_3$-Leu** probe to detect the LAP enzyme in 4T1 (mouse mammary carcinoma cells), HeLa (human cervical cancer cells) and SK-Mel-103 (human melanoma cells) cell, which exhibit high endogenous LAP levels, within 15 min of incubation. A significant reduction in the probe's fluorescent signal was observed upon inhibition of the enzyme's activity in these cancer cells. The **NB-SO$_3$-Leu** fluorophore was modified with sulfonic groups to improve its solubility and facilitate its renal elimination, a crucial modification that not only improves the solubility of the compound in biological media but also contributes significantly to the reduction of systemic toxicity.

We believe that the same strategy could be used to generate new fluorogenic probes for easy and fast cancer detection. In fact, the NB-SO$_3$ fluorophore represents a versatile modular tool that can be adapted to monitor the activity of other cancer-related enzymes. We anticipate that such adaptive detection systems open a new window in the development of molecular sensors with potential applications in biomedicine for the non-invasive detection and monitoring of cancer, one of the leading causes of death worldwide.

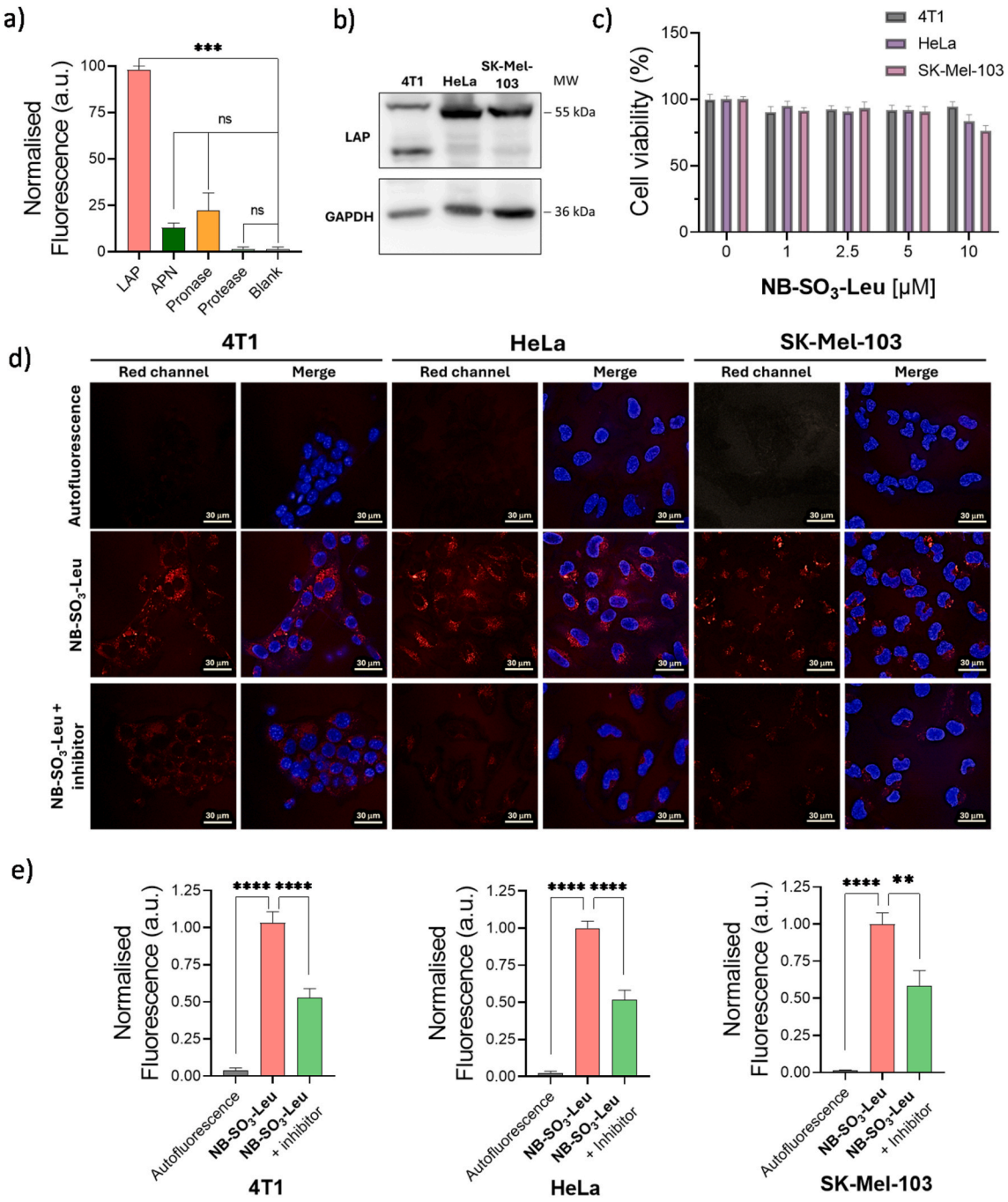

Fig. 4. (a) Fluorescence emission of **NB-SO_3-Leu** (5 μM) in DMEM with FBS in the presence of proteolytic enzymes as possible interferents at 660 nm (excitation at 630 nm). Error bars are expressed as 3σ for three independent experiments. Values are expressed as mean ± SEM. Statistical analysis was assessed by applying One-way ANOVA (***$p < 0.05$). (b) Western blot assay for LAP expression in 4T1, HeLa and SK-Mel-103 cells. (c) Cell viability in 4T1, HeLa and SK-Mel-103 cells incubated with different concentrations of **NB-SO_3-Leu** probe for 24 h. (d) Confocal images of not treated 4T1, HeLa and SK-Mel-103 cells incubated with **NB-SO_3-Leu** (10 μM), and 4T1, HeLa and SK-Mel-103 cells incubated with **NB-SO_3-Leu** (10 μM) + protease inhibitor cocktail. Cells were stained with **NB-SO_3-Leu** probe (red channel) and with Hoechst 33342 (blue channel) to identify the nucleus. (e) Fluorescence quantification of confocal images. Values are expressed as mean ± SEM of three independent experiments. Statistical analysis was assessed by applying One-way ANOVA followed by Tukey's test (****$p < 0.0001$, **$p < 0.01$). (For interpretation of the references to color in this figure legend, the reader is referred to the Web version of this article.)

CRediT authorship contribution statement

Marcia Domínguez: Writing – original draft, Validation, Methodology, Investigation. **David Azorín-Soriano:** Writing – review & editing, Validation. **Jessie García-Fleitas:** Validation. **Jennifer Soler-Beatty:** Validation. **Andrea Bernardos:** Writing – review & editing, Validation. **Alba García-Fernández:** Writing – review & editing, Supervision, Methodology, Investigation. **Juan F. Blandez:** Writing – review & editing, Supervision, Conceptualization. **Félix Sancenón:** Writing – review & editing, Supervision, Funding acquisition, Conceptualization. **Ramón Martínez-Máñez:** Writing – review & editing, Supervision, Funding acquisition, Conceptualization.

Declaration of competing interest

The authors declare that they have no known competing financial

interests or personal relationships that could have appeared to influence the work reported in this paper.

Acknowledgement

This research was supported by project PID2021-126304OB-C41 and PID2021-128141OB-C22 funded by MCIN/AEI/10.13039/501100011033/and by European Regional Development Fund - A way of doing Europe. This study was also supported by Generalitat Valenciana (CIPROM/2021/007). Thank the financial support from the FEDER found of European Union (IDIFEDER/2021/044). This research was supported by CIBER-Consorcio Centro de Investigación Biomédica en Red-(CB06/01/2012), Instituto de Salud Carlos III, Ministerio de Ciencia e Innovación. J. F. B. thanks to his postdoctoral fellowship APOSTD from Generalitat Valenciana (CIAPOS/2021/198).

Appendix. ASupplementary data

Supplementary data to this article can be found online at https://doi.org/10.1016/j.dyepig.2025.112827.

Data availability

Data will be made available on request.

References

[1] Brown E, Brunker J, Bohndiek SE. Photoacoustic imaging as a tool to probe the tumour microenvironment. Dis. Models Mech. 2019;12:dmm039636. https://doi.org/10.1242/dmm.039636.
[2] Fitzgerald RC, Antoniou AC, Fruk L, Rosenfeld N. The future of early cancer detection. Nat Med 2022;28:666–77. https://doi.org/10.1038/s41591-022-01746-x.
[3] Siddique S, Chow JC. Application of nanomaterials in biomedical imaging and cancer therapy. Nanomaterials 2020;10:1700. https://doi.org/10.3390/nano10091700.
[4] Bratulic S, Gatto F, Nielsen J. The translational status of cancer liquid biopsies. Regen. Eng. Transl. Med 2021;7:312–52. https://doi.org/10.1007/s40883-019-00141-2.
[5] Martin DR, Semelka RC. Health effects of ionising radiation from diagnostic CT. Lancet 2006;367:1712–4. https://doi.org/10.1016/S0140-6736(06)68748-5.
[6] Davies HE, Wathen CG, Gleeson FV. The risks of radiation exposure related to diagnostic imaging and how to minimise them. Br Med J 2011;342:d947. https://doi.org/10.1136/bmj.d947.
[7] Kobayashi H, Ogawa M, Alford R, Choyke PL, Urano Y. New strategies for fluorescent probe design in medical diagnostic imaging. Chem Rev 2010;110:2620–6. https://doi.org/10.1021/cr900263j.
[8] Hanash S M, Baik C S, Kallioniemi O. Emerging molecular biomarkers—Blood-based strategies to detect and monitor cancer. Nat Rev Clin Oncol 20211; 8:142-150. https://doi.org/10.1038/nrclinonc.2010.220.
[9] Wu L, Qu X. Cancer biomarker detection: recent achievements and challenges. Chem Soc Rev 2015;44:2963–97. https://doi.org/10.1039/C4CS00370E.
[10] Ahmad A, Imran M, Ahsan H. Biomarkers as biomedical bioindicators: approaches and techniques for the detection, analysis, and validation of novel biomarkers of diseases. Pharmaceutics 2023;15:1630. https://doi.org/10.3390/pharmaceutics15061630. 2023.
[11] Domínguez M, Meyer K, Sancenón F, Blandez JF, Serrano M, Martínez-Máñez R. A NIR fluorescent probe for the detection of renal damage based on overrepresentation of alanine aminopeptidase enzyme. ChemComm. 2023;59:2481–4. https://doi.org/10.1039/D2CC05408F.
[12] Lozano-Torres B, Blandez JF, Galiana I, Lopez-Domínguez JA, Rovira M, Paez-Ribes M, Gonzáles-Gualda E, Muñoz-Espín D, Serrano M, Sancenón F, Martínez-Máñez R. A two-photon probe based on naphthalimide-styrene fluorophore for the *In Vivo* tracking of cellular senescence. Anal Chem 2021;93:3052–60. https://doi.org/10.1021/acs.analchem.0c05447.
[13] Sarhadi VK, Armengol G. Molecular biomarkers in cancer. Biomolecules 2022;12:1021. https://doi.org/10.3390/biom12081021.
[14] Novak D, Utikal J. New biomarkers in cancers. Cancers 2021;13:708. https://doi.org/10.3390/cancers13040708.
[15] Peng S, Xiao F, Chen M, Gao H. Tumor-microenvironment-responsive nanomedicine for enhanced cancer immunotherapy. Adv Sci 2022;9:2103836. https://doi.org/10.1002/advs.202103836.
[16] Chu JC, Xiong J, Wong CT, Wang S, Tam DY, García-Fernández A, Martínez-Máñez R, Ng DK. Detection and elimination of senescent cells with a self-assembled senescence-associated β-Galactosidase-Activatable nanophotosensitizer. J Med Chem 2023;67:234–44. https://doi.org/10.1021/acs.jmedchem.3c01306.
[17] García-Fleitas J, García-Fernández A, Martí-Centelles V, Sancenón F, Bernardos A, Martínez-Máñez R. Chemical strategies for the detection and elimination of senescent cells. Acc Chem Res 2024;57:1238–53. https://doi.org/10.1021/acs.accounts.3c00794.
[18] Lozano-Torres B, Blandez JF, García-Fernández A, Sancenon F, Martínez-Máñez R. Lipofuscin labeling through biorthogonal strain-promoted azide-alkyne cycloaddition for the detection of senescent cells. FEBS J 2023;290:1314–25. https://doi.org/10.1111/febs.16477.
[19] Chu JC, Escriche-Navarro B, Xiong J, García-Fernández A, Martínez-Máñez R, Ng DK. β-Galactosidase-Triggered photodynamic elimination of senescent cells with a boron dipyrromethene-based photosensitizer. Adv Sci 2024;11:2401012. https://doi.org/10.1002/advs.202401012.
[20] Loudet A, Burgess K. BODIPY dyes and their derivatives: syntheses and spectroscopic properties. Chem Rev 2007;107:4891–932. https://doi.org/10.1021/cr078381n.
[21] Sameiro M, Gonçalves T. Fluorescent labeling of biomolecules with organic probes. Chem Rev 2009;109:190–212. https://doi.org/10.1021/cr0783840.
[22] Zeng L, Miller EW, Pralle A, Isacoff EY, Chang CJ. A selective turn-on fluorescent sensor for imaging copper in living cells. J Am Chem Soc 2006;128:10–1. https://doi.org/10.1021/ja055064u.
[23] Sun C, Du W, Wang B, Dong B, Wang B. Research progress of near-infrared fluorescence probes based on indole heptamethine cyanine dyes *In Vivo* and *In Vitro*. BMC Chem 2020;14:1–28. https://doi.org/10.1186/s13065-020-00677-3.
[24] Gosi M, Marepu N, Sunandamma Y. Cyanine-based fluorescent probe for cyanide ion detection. J Fluoresc 2021;31:1409–15. https://doi.org/10.1007/s10895-021-02771-8.
[25] Fan Y, Wu Y, Hou J, Wang P, Peng X, Ge G. Coumarin-based near-infrared fluorogenic probes: recent advances, challenges and future perspectives. Coord Chem Rev 2023;480:215020. https://doi.org/10.1016/j.ccr.2023.215020.
[26] Li J, Xie Y, Wang J, Wang L, Xia Y, Liu Y, Tan W. Activatable and self-monitoring hydrogen sulfide-based molecular senomorphics for visualized regulation of cellular senescence. CCS Chem 2023;5:2897–909. https://doi.org/10.31635/ccschem.023.202302714.
[27] Tian G, Zhang Z, Li H, Li D, Wang X, Qin C. Design, synthesis and application in analytical chemistry of photo-sensitive probes based on coumarin. Crit Rev Anal Chem 2021;51:565–81. https://doi.org/10.1080/10408347.2020.1753163.
[28] Wu R, Tian G, Zhang S, Zhang P, Lei X. A comprehensive review: versatile imaging probe based on chemical materials for biomedical applications. Appl Biochem Biotechnol 2024:1–28. https://doi.org/10.1007/s12010-024-05043-w.
[29] Siddique S, Chow JC. Application of nanomaterials in biomedical imaging and cancer therapy. Nanomaterials 2020;10:1700. https://doi.org/10.3390/nano10091700.
[30] Huang J, Xie C, Zhang X, Jiang Y, Li J, Fan Q, Pu K. Renal-clearable molecular semiconductor for second near-infrared fluorescence imaging of kidney dysfunction. Angew Chem Int Ed 2019;58:15120–7. https://doi.org/10.1002/anie.201909560.
[31] Zhu W, Kang M, Wu Q, Zhang Z, Wu Y, Li C, , et alTang BZ. Zwitterionic AIEgens: rational molecular design for NIR-II fluorescence imaging-guided synergistic phototherapy. Adv Funct Mater 2021;31:2007026. https://doi.org/10.1002/adfm.202007026.
[32] Li Q, Wen C, Yang J, Zhou X, Zhu Y, Zheng J, Cheng G, Bai J, Xu T, Ji J, Jiang S, Zhang L, Zhang P. Zwitterionic biomaterials. Chem Rev 2022;122:17073–154. https://doi.org/10.1021/acs.chemrev.2c00344.
[33] Jahanban-Esfahlan A, Ostadrahimi A, Jahanban-Esfahlan R, Roufegarinejad L, Tabibiazar M, Amarowicz R. Recent developments in the detection of bovine serum albumin. Int J Biol Macromol 2019;138:602–17. https://doi.org/10.1016/j.ijbiomac.2019.07.096.
[34] Li Y, Bai X, Yang D. Development and application of cationic nile blue probes in live-cell super-resolution imaging and specific targeting to mitochondria. *ACS central science*. ACS Cent Sci 2024;10:1221–30. https://doi.org/10.1021/acscentsci.4c00073.
[35] Rojas-Vázquez S, Lozano-Torres B, García-Fernández A, Galiana I, Pérez-Villalba A, Martí-Rodrigo P, Palop MJ, Domínguez M, Orzáez M, Sancenón F, Blandez JF, Fariñas I, Martínez-Máñez R. A renal clearable fluorogenic probe for *In Vivo* β-galactosidase activity detection during aging and senolysis. Nat Commun 2024;15:775. https://doi.org/10.1038/s41467-024-44903-1.
[36] Lozano-Torres B, Blandez JF, Galiana I, García-Fernández A, Alfonso M, Marcos MD, Orzez M, Sancenón F, Martínez-Máñez R. Real-time *in vivo* detection of cellular senescence through the controlled release of the NIR fluorescent dye nile blue. Angew Chem Int Ed 2020;59:15152–6. https://doi.org/10.1002/anie.202004142.
[37] Cheng P, Pu K. Molecular imaging and disease theranostics with renal-clearable optical agents. Nat Rev Mater 2021;6:1095–113. https://doi.org/10.1038/s41578-021-00328-6.
[38] Domínguez M, García-Fernández A, Martí-Centelles V, Sancenón F, Blandez JF, Martínez-Máñez R. Renal-clearable probes for disease detection and monitoring. Trends Biotechnol 2024. https://doi.org/10.1016/j.tibtech.2024.11.020.
[39] Holstein SA, Heckman CA, Davies FE, Morgan GJ, Gelius SS, Lehmann F. Aminopeptidases in cancer, biology and prospects for pharmacological intervention. Curr Cancer Drug Targets 2023;23:25–46. https://10.2174/1568009622666220623112605.
[40] Miettinen JJ, Kumari R, Traustadottir GA, Huppunen ME, Sergeev P, Majumder MM, Schepsky A, Gudjonsson T, Gorman PO, Slipicevic A, Anttila P, Silvennoinen R, Nupponen NN, Lehmann F, Heckman CA. Aminopeptidase expression in multiple myeloma associates with disease progression and sensitivity to Melflufen. Cancers 2021;13:1527. https://doi.org/10.3390/cancers13071527.
[41] Lozano-Torres B, García-Fernández A, Domínguez M, Sancenón F, Blandez JF, Martínez-Máñez R. β-Galactosidase-activatable nile blue-based NIR senoprobe for

the real-time detection of cellular senescence. Anal Chem 2022;95:1643–51. https://doi.org/10.1021/acs.analchem.2c04766.
[42] Arslan B, Bilici K, Demirci G, Almammadov T, Khan M, Sennaroglu A, Acar HY, Kolemen S. A leucine aminopeptidase activatable photosensitizer for cancer cell selective photodynamic therapy action. Dyes Pigments 2021;195:109735. https://doi.org/10.1016/j.dyepig.2021.109735.
[43] Zhou W, Liu YC, Ma QY, Feng GL, Zhang JW, Liu GJ, Zhang Y, Xing GW. AIE-Active lysosome-targeted fluorescent organic nanoparticles for leucine aminopeptidase-activatable fluorescent imaging and precision photodynamic therapy potential. Dyes Pigments 2024;221:111781. https://doi.org/10.1016/j.dyepig.2023.111781.
[44] Wu X, Deng Y, Xu Y, Kang H, Hu JJ, Yoon J, Liang G. Activatable fluorescence and bio/chemiluminescence probes for aminopeptidases: from design to biomedical applications. Adv Mater 2024;36:2409893. https://doi.org/10.1002/adma.202409893.
[45] Li X, Yin C, Zhang L, Huo F. Research progress of small molecule fluorescent probes for liver cancer related enzymes. Dyes Pigments 2023;219:111631. https://doi.org/10.1016/j.dyepig.2023.111631.
[46] Jeong H, Wu X, Lee JS, Yoon J. Recent advances in enzyme-activated NIR fluorescent probes for biological applications. TrAC, Trends Anal Chem 2023;168:117335. https://doi.org/10.1016/j.trac.2023.117335.
[47] Chen Y. Fluorescent probes for detection and bioimaging of leucine aminopeptidase. Mater Today Chem 2020;15:100216. https://doi.org/10.1016/j.mtchem.2019.100216.
[48] Li ZJ, Wang CY, Xu L, Zhang ZY, Tang YH, Qin TY, Wang YL. Recent progress of activity-based fluorescent probes for imaging leucine aminopeptidase. Biosensors 2023;13:752. https://doi.org/10.3390/bios13070752.
[49] Matsui M, Fowler JH, Walling LL. Leucine aminopeptidases: diversity in structure and function. Biol Chem 2006;387:1535–44. https://doi.org/10.1515/BC.2006.191.
[50] Grembecka J, Mucha A, Cierpicki T, Kafarski P. The Most potent organophosphorus inhibitors of leucine aminopeptidase. Structure-based design, chemistry, and activity. J Med Chem 2003;46:2641–55. https://doi.org/10.1021/jm030795v.
[51] Tsujimoto M, Goto Y, Maruyama M, Hattori A. Biochemical and enzymatic properties of the M1 family of aminopeptidases involved in the regulation of blood pressure. Heart Fail Rev 2008;13:285–91. https://doi.org/10.1007/s10741-007-9064-8.
[52] Kondo C, Shibata K, Terauchi M, Kajiyama H, Ino K, Nomura S, Nawa A, Miztutani Sh, Kikkawa F. A novel role for placental leucine aminopeptidase (P-LAP) as a determinant of chemoresistance in endometrial carcinoma cells. Int. J. Cancer Manag 2006;118:1390–4. https://doi.org/10.1002/ijc.21509.
[53] Zhan C, Cheng J, Li B, Huang S, Zeng F, Wu S. A fluorescent probe for early detection of melanoma and its metastasis by specifically imaging tyrosinase activity in a mouse model. Anal Chem 2018;90:8807–15. https://doi.org/10.1021/acs.analchem.8b00594.
[54] Zeng Z, Liew SS, Wei X, Pu K. Hemicyanine-based near-infrared activatable probes for imaging and diagnosis of diseases. Angew Chem 2021;133:26658–79. https://doi.org/10.1002/anie.202107877.
[55] Yoon HY, Shim SH, Baek LJ, Hong JI. Small-molecule probe using dual signals to monitor leucine aminopeptidase activity. Bioorg Med Chem Lett 2011;21:2403–5. https://doi.org/10.1016/j.bmcl.2011.02.068.
[56] Gong Q, Shi W, Li L, Ma H. Leucine aminopeptidase May contribute to the intrinsic resistance of cancer cells toward cisplatin as revealed by an ultrasensitive fluorescent probe. Chem Sci 2016;7:788–92. https://doi.org/10.1039/C5SC03600C.
[57] Zhou Z, Wang F, Yang G, Lu C, Nie J, Chen Z, , et alZhu WH. A ratiometric fluorescent probe for monitoring leucine aminopeptidase in living cells and zebrafish model. Anal Chem 2017;89:11576–82. https://doi.org/10.1021/acs.analchem.7b02910.
[58] Wu B, Lin Y, Li B, Zhan C, Zeng F, Wu S. Oligo (ethylene glycol)-functionalized squaraine fluorophore as a near-infrared-fluorescent probe for the *In Vivo* detection of diagnostic enzymes. Anal Chem 2018;90:9359–65. https://doi.org/10.1016/j.dyepig.2021.109284.
[59] Huang Y, Qi Y, Zhan C, Zeng F, Wu S. Diagnosing drug-induced liver injury by multispectral optoacoustic tomography and fluorescence imaging using a leucine-aminopeptidase-activated probe. Anal Chem 2019;91:8085–92. https://doi.org/10.1021/acs.analchem.9b00107.
[60] Wang B, Chen Z, Cen X, Liang Y, Tan L, Liang E, , et alCheng K. A highly selective and sensitive chemiluminescent probe for leucine aminopeptidase detection *in vitro, in vivo* and in human liver cancer tissue. Chem Sci 2022;13:2324–30. https://doi.org/10.1039/D1SC06528A.
[61] Zhong R, Jiang R, Zeng J, Gong X, Yang X, He L, , et alCheng D. Enhancing the selectivity of leucine aminopeptidase near-infrared fluorescent probes for assisting in surgical tumor resection. Anal Chem 2023;95:2428–35. https://doi.org/10.1021/acs.analchem.2c04587.
[62] Liu Y, Liu X, Liu Q, Li D, Cheng D, He L. Engineering a highly selective leucine aminopeptidase near-infrared fluorescence probe for early diagnosis of diabetic nephropathy. Sensor Actuator B Chem 2024;402:135127. https://doi.org/10.1016/j.snb.2023.135127.
[63] Liu HW, Chen L, Xu C, Li Z, Zhang H, Zhang XB, Tan W. Recent progresses in small-molecule enzymatic fluorescent probes for cancer imaging. Chem Soc Rev 2018;47:7140–80. https://doi.org/10.1039/C7CS00862G.
[64] Tracy TS. Enzyme kinetics. Drug metabolism in drug design and development: basic concepts and practice 2008;4:89–112.
[65] Li R, Guo J, Duan Y, Liu X, Gui L, Xu Y, Kong X, Li Y, Chen H, Yuan Z. Monitoring inflammation-cancer progression by cell viscosity, polarity and leucine aminopeptidase using multicolor fluorescent probe. Chem Eng J 2022;435:135043. https://doi.org/10.1016/j.cej.2022.135043.
[66] Alonso IP, Méndez LR, García FA, Valdés-Tresanco ME, Bosch RA, Perera WH, Sánchez YA, Bergado G, Sánchez-Ramírez B, Charli JL. Bufadienolides preferentially inhibit aminopeptidase N among Mammalian metallo-aminopeptidases; relationship with effects on human melanoma MeWo cells. Int J Biol Macromol 2023;229:825–37. https://doi.org/10.1016/j.cej.2022.135043.
[67] Zhang H, Mao Z, Wang F, Yang G, Zhang Y, Zhang X. Multi-dimensional imaging of endogenous leucine aminopeptidase via fast response fluorescent read-out probe. Dyes Pigments 2021;187:109145. https://doi.org/10.1016/j.dyepig.2021.109145.